Integrated description of protein dynamics from room-temperature X-ray crystallography and NMR

R. Bryn Fenwick[a], Henry van den Bedem[b], James S. Fraser[c], and Peter E. Wright[a,1]

[a]Department of Integrative Structural and Computational Biology and the Skaggs Institute for Chemical Biology, The Scripps Research Institute, La Jolla, CA 92037; [b]Joint Center for Structural Genomics, Stanford Synchrotron Radiation Lightsource, Stanford, CA 94025; and [c]Department of Bioengineering and Therapeutic Sciences, University of California, San Francisco, CA 94158

Contributed by Peter E. Wright, December 18, 2013 (sent for review December 3, 2013)

Detailed descriptions of atomic coordinates and motions are required for an understanding of protein dynamics and their relation to molecular recognition, catalytic function, and allostery. Historically, NMR relaxation measurements have played a dominant role in the determination of the amplitudes and timescales (picosecond–nanosecond) of bond vector fluctuations, whereas high-resolution X-ray diffraction experiments can reveal the presence of and provide atomic coordinates for multiple, weakly populated substates in the protein conformational ensemble. Here we report a hybrid NMR and X-ray crystallography analysis that provides a more complete dynamic picture and a more quantitative description of the timescale and amplitude of fluctuations in atomic coordinates than is obtainable from the individual methods alone. Order parameters (S^2) were calculated from single-conformer and multiconformer models fitted to room temperature and cryogenic X-ray diffraction data for dihydrofolate reductase. Backbone and side-chain order parameters derived from NMR relaxation experiments are in excellent agreement with those calculated from the room-temperature single-conformer and multiconformer models, showing that the picosecond timescale motions observed in solution occur also in the crystalline state. These motions are quenched in the crystal at cryogenic temperatures. The combination of NMR and X-ray crystallography in iterative refinement promises to provide an atomic resolution description of the alternate conformational substates that are sampled through picosecond to nanosecond timescale fluctuations of the protein structure. The method also provides insights into the structural heterogeneity of nonmethyl side chains, aromatic residues, and ligands, which are less commonly analyzed by NMR relaxation measurements.

B factor | nuclear magnetic resonance | atomic displacement parameters | Lipari-Szabo

The conformational dynamics of proteins play an important role in their functional mechanisms, influencing such diverse processes as conformational selection in molecular recognition (1), catalytic function (2, 3), and allosteric regulation (4). To understand the atomic motions that underlie protein dynamics and configurational entropy, it has become increasingly important to study both the timescales of motions and how those motions are manifest in the structure as coordinate changes. Two complementary methods are high-resolution X-ray crystallography and NMR spectroscopy, which provide coordinate precision and probe motions within well-defined timescales, respectively. The combination of X-ray and NMR data has thus far been limited to coordinate refinement because no rigorous framework exists to connect the coordinates and motional timescales (5–7).

Proteins are not rigid and constantly sample distinct conformational substates (8). The coordinates derived from X-ray diffraction are accompanied by atomic displacement parameters or B factors that are related to the displacements of the atoms from their mean positions (9). B factors can contain varying contributions, which include but are not limited to, model errors, invalid restraints, and dynamic and static disorder. Dynamic disorder arises from temperature-dependent fluctuations in the atomic positions and has been observed to be the major contributor to the B factor (10). In contrast, static disorder, also referred to as lattice disorder, arises from crystal imperfections where various distinct noninterconverting conformations and orientations of molecules exist within the crystal lattice. Although the effects of static and dynamic disorder are the same, i.e., they increase the value of the B factor, it has long been hypothesized that their relative contributions can be estimated by comparing data collected at different temperatures. One consequence of static and dynamic disorder in crystals is that the comparison of dynamics from crystallographic B factors and NMR order parameters has met with mixed results. Powers et al. (11) compared B factors and NMR backbone order parameters and found poor qualitative agreement. More recently the use of contact models (12, 13), normal mode analysis (14–16), restrained molecular dynamics (17), and ensembles of high-sequence similarity (18) have been shown to give better agreement between order parameters and X-ray crystal structures. These methods, however, are limited in use as they rely heavily on empirical relations, the accuracy of force field parameterization, or on the availability of many homologous structures. Despite the poor correlation observed between B factors, coordinates, and NMR order parameters in previous studies, there is mounting evidence from both NMR (19) and neutron scattering spectroscopy (20) that picosecond–nanosecond (ps–ns) motions observed in solution are the same as those observed in the solid state. Agarwal et al. (21) suggest that motions on the ps–ns timescale dominate motional amplitudes for globular proteins. For the SH3 domain of α-spectrin, ^{15}N backbone and

Significance

Most proteins are inherently flexible and their dynamics play a central role in their biological functions. A molecular level understanding of protein function and mechanism requires an accurate description of the atomic coordinates in both time and space. Here we show, through studies of the enzyme dihydrofolate reductase, that multiconformer models derived from room-temperature X-ray crystallographic data can be used synergistically with nuclear magnetic resonance relaxation measurements to provide a detailed description of both the amplitude and timescale of fluctuations in atomic coordinates. This hybrid approach provides a more complete description of protein dynamics than can be obtained from either method alone. The room-temperature crystallographic ensemble accurately reflects the picosecond–nanosecond motions of the protein backbone and side chains.

Author contributions: R.B.F. and P.E.W. designed research; R.B.F., H.v.d.B., and J.S.F. performed research; R.B.F., H.v.d.B., J.S.F., and P.E.W. analyzed data; and R.B.F. and P.E.W. wrote the paper.

The authors declare no conflict of interest.

Data deposition: The atomic coordinates and structure factors have been deposited in the Protein Data Bank, www.pdb.org (PDB ID codes 4NX6 and 4NX7).

[1]To whom correspondence should be addressed. E-mail: wright@scripps.edu.

This article contains supporting information online at www.pnas.org/lookup/suppl/doi:10.1073/pnas.1323440111/-/DCSupplemental.

side-chain dynamics are the same in solution and the solid state (21, 22). Recently, similar results were reported for ubiquitin and showed good agreement between solution-state ps–ns order parameters and those measured in the crystalline form by solid-state NMR (23). Motions on the ps–ns timescale now are routinely measured for backbone and for methyl-containing side chains by NMR relaxation experiments. This allows the study of motional timescales throughout the protein, most commonly; through the backbone NH (S^2) and methyl axis (S^2_{axis}) order parameters.

For high-resolution X-ray data sets, dynamic information can potentially be extracted from multiple conformations modeled into the electron density. In the recently developed qFit approach, a small number of conformations are locally fitted to the electron density for each protein residue (24). The resulting multiconformer structural model can then be used to map allosteric pathways and other dynamic processes within the protein (25).

Here we use the enzyme dihydrofolate reductase (DHFR), for which the connection between dynamics and function has been extensively studied, to test firstly if qFit conformational ensembles of the DHFR:folate:NADP$^+$ complex are representative of the fast timescale motions described by NMR order parameters in solution, and secondly to test if regions of DHFR that do not fit well can be explained by packing in the crystal lattice. We find that a simple physical model that incorporates the B factor can accurately predict the backbone and side-chain dynamics of DHFR on the ps–ns timescale. Regions of the protein involved in crystal lattice contacts are affected by motional dampening, whereas residues that are affected by static disorder can be identified by their insensitivity to temperature change.

Theory

The order parameter S^2 can be expressed as the sum of the second-order spherical harmonics

$$S^2 = \frac{4\pi}{5}\sum_{m=-2}^{2} Y^*_{2m}(\theta,\phi)Y_{2m}(\theta,\phi), \qquad [1]$$

where $Y_{2m}(\theta,\phi)$ are the second-order spherical harmonics of the bond vector with the direction defined by θ and ϕ in the fixed frame (26). Brüschweiler and Wright (27) recognized that this could be expressed as the sum of the variances of the spherical harmonics (σ^2) as

$$1 - S^2 = \frac{4\pi}{5}\sum_{m=-2}^{2}\sigma^2_{Y_{2m}}. \qquad [2]$$

This form clearly demonstrates the relationship between S^2 and the B factor, expressed as the sum of the variances of the first-order spherical harmonics modulated by the distance (r) from the equilibrium position (27).

$$\frac{3}{8\pi^2}B = \frac{4\pi}{3}\sum_{m=-1}^{1}\sigma^2_{rY_{1m}}. \qquad [3]$$

The B factor reports on the variances of the distance-modulated first-order spherical harmonics of individual atom positions, whereas S^2 reports on the variances of the second-order spherical harmonics of atom pairs. Although not explicitly stated in the original paper (27), an expression for the calculation of S^2_B from the B factor naturally follows as

$$S^2_B = 1 - \frac{3}{8\pi^2}B, \qquad [4]$$

where B is the B factor of the heavy atom.

In cases where averaging occurs over multiple conformational states, the value of S^2 can be calculated as (27)

$$S^2 = \sum_{i=1}^{N}\sum_{j=1}^{N} p_i p_j\left[\delta_{ij}S^2_B + (1-\delta_{ij})P_2(\cos\theta_{ij})\right], \qquad [5]$$

where the p_i and p_j are the local populations of conformational states i and j, S^2_B is the order parameter defined in Eq. **4**, and P_2 is the second-order Legendre polynomial of the angle (θ_{ij}) between the bond vector for states i and j, and δ_{ij} is the Kronecker delta.

The 3D isotropic B factor (Eq. **4**) overestimates the amplitude of motion because it contains components that represent translational motions parallel to and transverse to the bond vector (Fig. 1), which have no effect on NMR relaxation. The NMR order parameter is sensitive only to angular fluctuations of the bond vector, represented by the red cone in Fig. 1. Assuming for the moment that the position of atom v is fixed, the amplitude of the bond vector fluctuations is related to the root-mean-square displacement ($\bar{u}$) of the atomic coordinates of atom u in a direction transverse to the bond vector. The order parameter is then given by

$$S^2_{\text{ortho},u} = P_2(\cos\bar{\alpha})^2, \qquad [6]$$

where $\tan(\bar{\alpha}) = \bar{u}/r$, $\bar{u}$ is the root-mean-square displacement of atom u from its mean position, and r is the u–v bond length. In terms of the B factor,

$$S^2_{\text{ortho},u} = 1 - \frac{1}{8\pi^2}B_u. \qquad [7]$$

Because fluctuations in the position of atom v also influence the angle $\bar{\alpha}$, the B factor of atom v must also be taken into account in calculating the order parameter

$$S^2_{\text{ortho},uv} = 1 - \frac{B_u + B_v}{8\pi^2}. \qquad [8]$$

To compare the order parameters measured from NMR spectroscopy with the motional amplitudes in the qFit ensembles and single-conformer X-ray structures, we developed the following model. Because NMR relaxation is associated with angular fluctuations of bond vectors, and is insensitive to translational motions, an angular order parameter (S^2_{angular}) was calculated from the qFit ensembles and was corrected with an orthogonal order parameter (S^2_{ortho}) that accounts for the additional motion within each state represented by the B factor. The relationship between

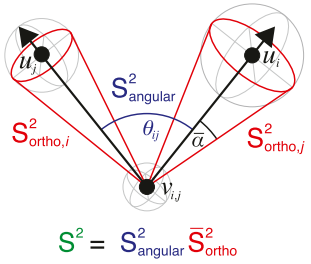

Fig. 1. Motions reported by the order parameter are represented in the qFit ensembles as the product of two components for the pair of atoms u and v. The angular component (blue) that is defined by θ_{ij} is sensitive to multiple states within the structural model, and the orthogonal component (red) accounts for the motion within each state. Note that the orthogonal component of the order parameter can differ between states when the atoms involved have different B factors in each state.

the orthogonal and angular order parameters is shown in Fig. 1 and illustrates how the orthogonal order parameter accounts for the local motions within each discrete state. The order parameter from the X-ray structural models was calculated as

$$S^2 = S^2_{\text{ortho}} S^2_{\text{angular}}, \quad [9]$$

where the orthogonal order parameter accounts for motions encoded in the isotropic B factors of a pair of bonded atoms. The orthogonal order parameter was calculated following ref. 27, where the motion of the two atoms was assumed to be uncorrelated (28) to give the final form as

$$S^2_{\text{ortho}} = 1 - \sum_{i=1}^{N} p_i \left[\frac{B_{i,u} + B_{i,v}}{8\pi^2} \right], \quad [10]$$

where $B_{i,u}$ and $B_{i,v}$ are the B factors of atoms u and v of conformational state i, p_i is the occupancy (probability), obtained during model generation, of state i, and N is the number of states. Occupancies, together with coordinates and B factors obtained from the qFit algorithm, were refined until convergence according to the protocol described in van den Bedem et al. (24, 25). Eq. **10** defines (S^2_{ortho}) as the sum of (S^2_{ortho}) over the different conformations weighted by their respective occupancies. To calculate the order parameters for NH bonds in which the hydrogen atom is much lighter than the nitrogen atom, the riding model, where the lighter atom is considered to "ride" on the heavier atom, is appropriate (28). In using the riding model to describe the motion of the amide hydrogen, the sum of $B_{i,u}$ and $B_{i,v}$ simplifies to the amide proton B factor ($B_{i,u}$) because the hydrogen B factor already includes the contribution from the fluctuations of the amide nitrogen. During model refinement the amide proton B factor was obtained using the riding model, by multiplying the nitrogen B factor by 1.2. Note that the amide proton B factor can also be calculated from the heavy atom B factors in the peptide plane using the 1D Gaussian axial fluctuation (1D-GAF) model (27), which describes the peptide plane as it samples rotations about the C^{α}_{i-1}–C^{α}_{i} axis via the crankshaft motion, which is related to the γ-motion of the 3D-GAF model (29).

The angular order parameter is the standard order parameter defined as (26, 27)

$$S^2_{\text{angular}} = \sum_{i,j=1}^{N} p_i p_j \left[P_2(\cos\theta_{ij}) \right], \quad [11]$$

where N is the number of states, p is the probability of a given state, and P_2 is the second-order Legendre polynomial of the angle between the bond vectors of atoms u and v for states i and j.

The calculated order parameter for single-conformer structural models becomes unphysical (negative) when the sum of the two B factors approaches $8\pi^2$ Å^2 (~79 Å^2). This limits the applicability of Eq. **10** to high-resolution X-ray structures. However, for data with resolutions better than 1.7 Å, the range at which qFit is most effective, B factors are usually sufficiently small and the model presented here applies. At low resolutions, the inability to model alternative conformations will lead to excessive heterogeneity and large B factors for a single conformer and the inability to separate S^2_{ortho} and S^2_{angular}. A symptom of the

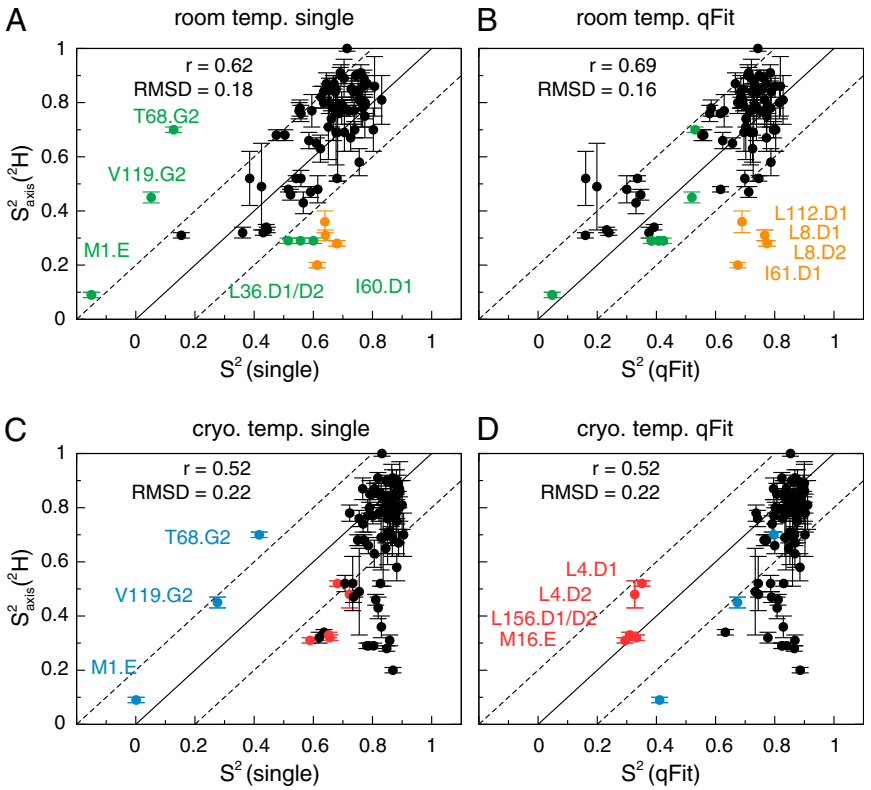

Fig. 2. Correlation plots of experimental S^2_{axis} for methyl groups with values calculated from a single structure (*A*) and a multistate qFit model (*B*) at room temperature. Residues in green improve their fit to the experimental data in the qFit model, whereas residues in orange appear as outliers in both single and qFit models. Dashed lines indicate ±0.2 from ideal agreement. For comparison, *C* and *D* show order parameters for a crystal at cryogenic temperature, single and multistate qFit models, respectively. Residues in blue improve agreement in the qFit model, whereas residues in red appear to have the same order parameters at both temperatures.

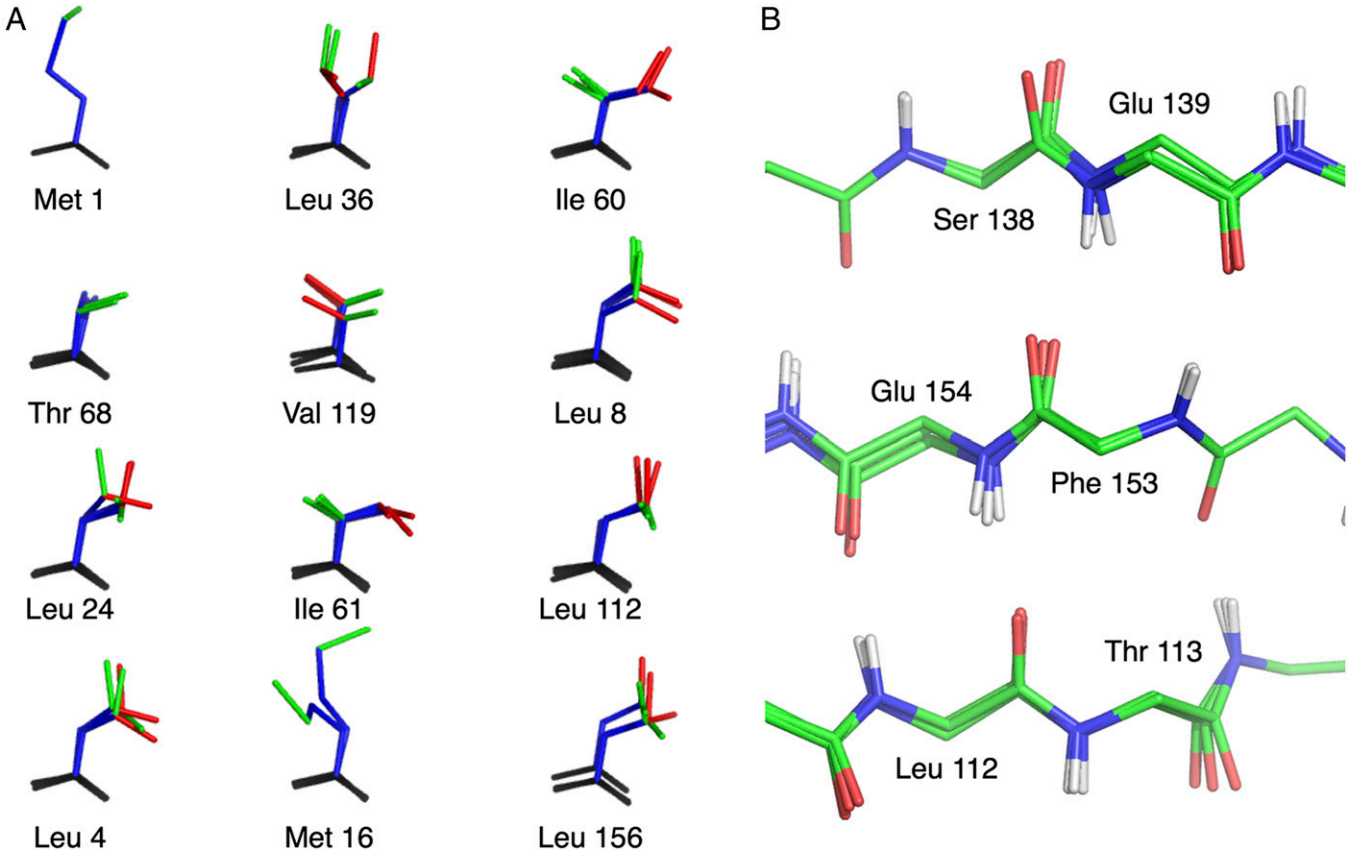

Fig. 3. (*A*) Conformational states observed for representative methyl-containing residues. The backbone is shown as black, side-chain bonds in blue, and bonds to the methyls are identified as green and red. (*B*) Anharmonic motions of the peptide planes in the central β-sheet of the room-temperature qFit multiconformer model.

failure of the model can be seen in Fig. 1*A*, where the predicted order parameter for M1 is negative (B_{sum} = 90.8 Å^2).

Results

Backbone and methyl side-chain order parameters were calculated from single-conformer and multiconformer qFit models determined from cryogenic and room-temperature X-ray diffraction data for the E:FOL:NADP$^+$ complex of *Escherichia coli* DHFR. The refinement of the single-conformer structures is described in *Materials and Methods*; the refinement of the cryo- (PDB ID code 4KJJ) and room-temperature (PDB ID code 4KJK) multiconformer structures has previously been reported (25). The X-ray–derived order parameters were then compared with backbone NH (S^2) and methyl axis (S^2_{axis}) order parameters derived from ^{15}N and ^{2}H relaxation experiments (30, 31).

Side-Chain Methyl Dynamics. The dynamics of methyl groups are of particular interest because they are prevalent in the core of proteins and in hydrophobic pockets that bind ligands. Methyl order parameters for fluctuations on the ps–ns timescale take values between zero for unrestricted motion and 1 for a fixed orientation and can be determined from either ^{13}C or ^{2}H relaxation measurements (32, 33). The S^2_{axis} order parameter describes the motion of the C_{methyl}–C bond.

Inspection of the room-temperature qFit multiconformer model of the E:FOL:NADP+ complex reveals the presence of disorder for methyl groups and other side chains, both in the core and on the surface of the protein. Eq. **9** was used to calculate S^2_{axis} for the structural models. In Fig. 2*A* the experimental S^2_{axis} values derived from deuterium relaxation (30) are compared with order parameters calculated from a single-conformer model fitted to the electron density obtained from room-temperature diffraction data at a resolution of 1.35 Å. Good agreement was observed between the measured S^2_{axis} values and those calculated from the single structures using the isotropic B factors to represent motion in the crystal (r = 0.62 and rmsd = 0.18). In Fig. 2*B* we show the comparison of the measured S^2_{axis} with values calculated from the qFit multiconformer model fitted to the same electron density, where as many as three states are modeled for any given residue (PDB ID code 4KJK). The agreement between experimental S^2_{axis} values and those calculated from the single structure and the qFit ensemble (r = 0.69 and rmsd = 0.16) was comparable, although some differences were apparent. The qFit model fit order parameters for three outliers, M1, T68, and V119 (Fig. 2*A*), better than the single-conformer model. For T68 and V119, the B factor in the single-conformer model overestimates the motion (smaller S^2_{axis}), which the qFit model reveals is predominantly translational in nature and therefore does not contribute to methyl spin relaxation. In contrast, order parameters for residues L36 and I60 are underestimated using the single-conformer model. These side chains were modeled with multiple distinct rotamers in the qFit multiconformer model (Fig. 3*A*), which increased the angular fluctuations and resulted in lower predictions of S^2_{axis}, in closer agreement with the experimental values.

The poorer agreement between the experimental values and S^2_{axis} values calculated from single-conformer models originates from the difficulty in estimating the angular contribution of the motion from the B factor alone when multiple rotamer or translational states exist. In Fig. 3*A* we show the qFit representation for some illustrative residues. In cases like V119, where

the single-conformer model underestimated the order parameter, it is clear that the B factor exaggerated the angular fluctuations because substantial translational motion is present. In cases like L36, where the single structure overestimated the order parameter, calculation of S^2_{axis} from the B factor alone diminished the angular contribution from rotamer averaging. Note that the presence of ns timescale motions, potentially associated with rotamer transitions, will influence the generalized S^2_{axis} parameter used in this work and could also weaken the correlation between calculated and experimental order parameters (34). This is less of an issue for the NH order parameters analyzed below. The qFit models are expected to perform better than the single-conformer models for two reasons. Firstly, the qFit models allow the translational components of motions, which have the effect of reducing the calculated order parameter, to be removed. Secondly, qFit models more accurately describe anharmonic and multimodal distributions of rotamer states because each of the states is modeled using a unique B factor. The visual inspection of the side chains in Fig. 3 reveals the presence of translational motion with distinct anharmonicity, i.e., nonsymmetric motional envelope. The anharmonicity is manifested as translational states of V119 and L156 side chains and as multiple rotamer states for residues like L36 and M16.

The improved agreement observed for residue 1 when the qFit model is used to calculate S^2_{axis} (Fig. 2 *A* and *B*) suggests that models built with qFit can indirectly improve the fit to the dynamic data, even if the residue is modeled with a single conformation. During the qFit model building, multiple states of neighboring residues caused a reduction in the fitted B factors for the side chain of M1, which in turn increased S^2_{ortho} and brought the calculated order parameter into better quantitative agreement with experiment. Three other residues L8, I61, and L112 were not fit well by either of the room-temperature structural models, with deviations of more than 0.2 between the experimental and calculated S^2_{axis} values. The reason for this discrepancy is discussed below.

We also calculated S^2_{axis} for single-conformer and qFit models built in the electron density from diffraction data measured at cryogenic temperature at 1.15 Å resolution. In Fig. 2 *C* and *D* we compare S^2_{axis} calculated from these models to the experimental values of S^2_{axis} measured at room temperature. In general, the room-temperature models display lower calculated order parameters than the cryogenic temperature models, as would be expected due to damping of thermal motions at cryogenic temperatures. For both the single-conformer and the qFit models, the S^2_{axis} values calculated from the low-temperature structures cluster around a value of 0.8 for the majority of the methyls.

A comparison of S^2_{axis} predictions from the original model derived from Brüschweiler and Wright's equations 4 and 5 (27), the contact model of Ming and Brüschweiler (13), and from Eqs. **9**–**11** of the current study, is presented in Fig. S1. The earlier model of Brüschweiler and Wright performed worse than the model used in the present work, whereas the agreement with the contact mode of Ming and Brüschweiler is comparable to the model presented here. However, the temperature sensitivity of the order parameters is not captured by the contact models (Fig. S1).

Backbone Amide Dynamics. To compare with ^{15}N relaxation measurements, we calculated NH order parameters from the structural models, with a slight modification of Eq. **10** to account for riding motion of the amide group on the peptide plane. For room-temperature diffraction data, the amide ^{15}N order parameters

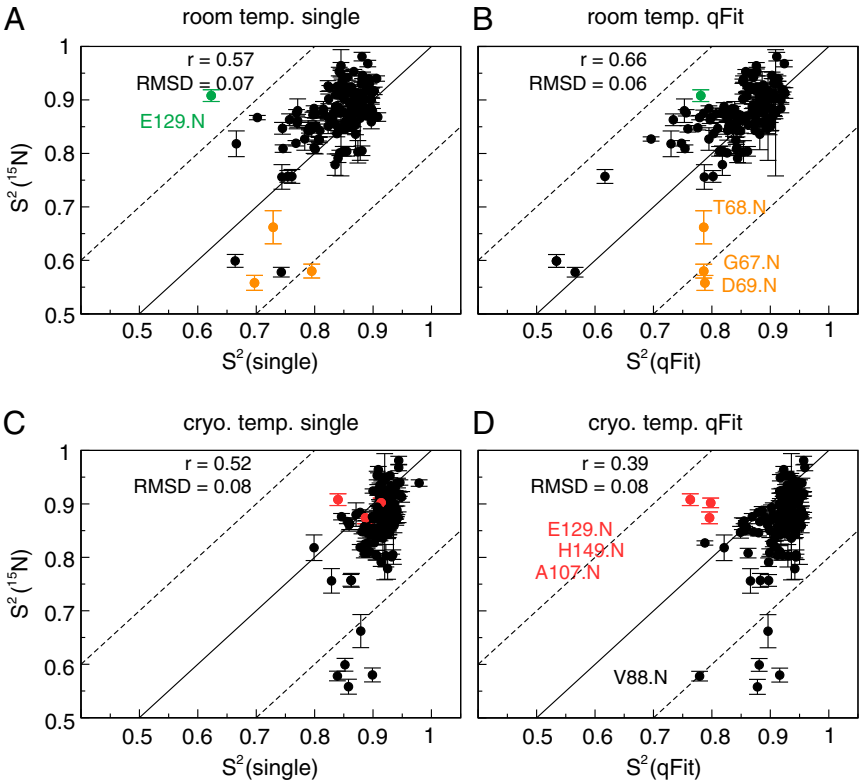

Fig. 4. Correlation plots of experimental NH S^2 with values calculated from a single structure (*A*) and a multistate qFit model (*B*) at room temperature. The residue in green improves in fit whereas orange points appear as outliers in both single and qFit models. Dashed lines indicate ±0.2 from ideal agreement. For comparison, *C* and *D* show order parameters for a crystal at cryogenic temperature, single and multistate qFit models, respectively. Residues in red appear to have the similar or increased order parameters at the cryogenic temperature.

calculated from both the single-conformer ($r = 0.61$ and rmsd = 0.06) and qFit models ($r = 0.61$ and rmsd = 0.06) fit the experimental relaxation data well, with the exception of three residues (67, 68, and 69) whose motion appears to be restricted in the crystal lattice (Fig. 4 *A* and *B*) The NH order parameters calculated from the cryogenic crystallographic data indicate decreased flexibility of the backbone relative to the room-temperature structures. The backbone order parameters calculated from the room-temperature diffraction data cover the range of values between 0.5 and 0.95, whereas the order parameters from the low-temperature crystal data cluster around the value of 0.90. This is in contrast with the methyl S^2_{axis} order parameters, which range between zero and 0.80 at room temperature and cluster around 0.85 at cryogenic temperatures. The change in order parameters shows that much of the motion of the backbone amides and side chains is quenched at cryogenic temperatures. As for the methyl side chains, the NH order parameters calculated using a contact model were insensitive to the temperature change (Fig. S2). The original Brüschweiler and Wright model (27) performed poorly, greatly overestimating the amplitude of the backbone NH motions (Fig. S2).

Inspection of the backbone coordinates from the room-temperature qFit multiconformer models reveals that the anisotropy and anharmonicity of motion in the backbone is even more pronounced than for the side chains. Crankshaft motion of the peptide plane, i.e., rotation of the peptide plane about the C^{α}_{i-1}–C^{α}_{i} axis, can be clearly observed, whereas motions between neighboring peptide planes appear to be coupled through hydrogen bonds (Fig. 3B and Fig. S3). These motions were manifest in the qFit multiconformer model as peptide plane rotation in pairs of residues that are connected by hydrogen bonds in α-helices and between adjacent strands in the β-sheets. The crankshaft motion of peptide planes in the secondary structure elements is strikingly similar to the γ-motions observed in the 3D-GAF analysis of backbone dynamics in a domain of streptococcal protein G (35).

Static and Dynamic Disorder. To estimate the static and dynamic contributions to disorder we compared the $S^2_{angular}$ and S^2_{ortho} components of the calculated order parameter as a function of temperature (Fig. 5). Residues that are likely affected by static disorder can be identified from the temperature independence of the $S^2_{angular}$ value. In Fig. 5 *A* and *C* we show the temperature dependence of the angular component ($S^2_{angular}$) of the methyl and NH order parameters. At the cryogenic temperature (100 K), which is well below the glass transition for proteins (36), five methyl groups of three residues (L4, M16, and L156) are disordered at both room and cryogenic temperatures and exhibit $S^2_{angular}$ values near 0.4 at both temperatures (Fig. 5*A*). This result could indicate static disorder, where the side chains in some unit cells are trapped in an alternative conformation and do not interconvert within the crystal lattice in a temperature-dependent manner. Alternatively, there may be a high barrier for exchange between the different conformations, such that the higher viscosity of the glassy water at cryogenic temperatures effectively arrests the interconversion (37). L4 and L156 are positioned at the core of the protein whereas M16 is close to a crystal contact. The static disorder observed for these residues may arise through trapping at the time of lattice formation during crystallization. Alternatively, these residues may exchange between different conformations within the crystal, and the cryocooling process simply traps this distribution. Whatever the mechanism, the observation implies that less than 6% of the observed methyl-containing residues are affected by this type of disorder. This suggests that static disorder associated with intermolecular contacts in the crystal lattice plays a minor role in protein crystals at room temperature.

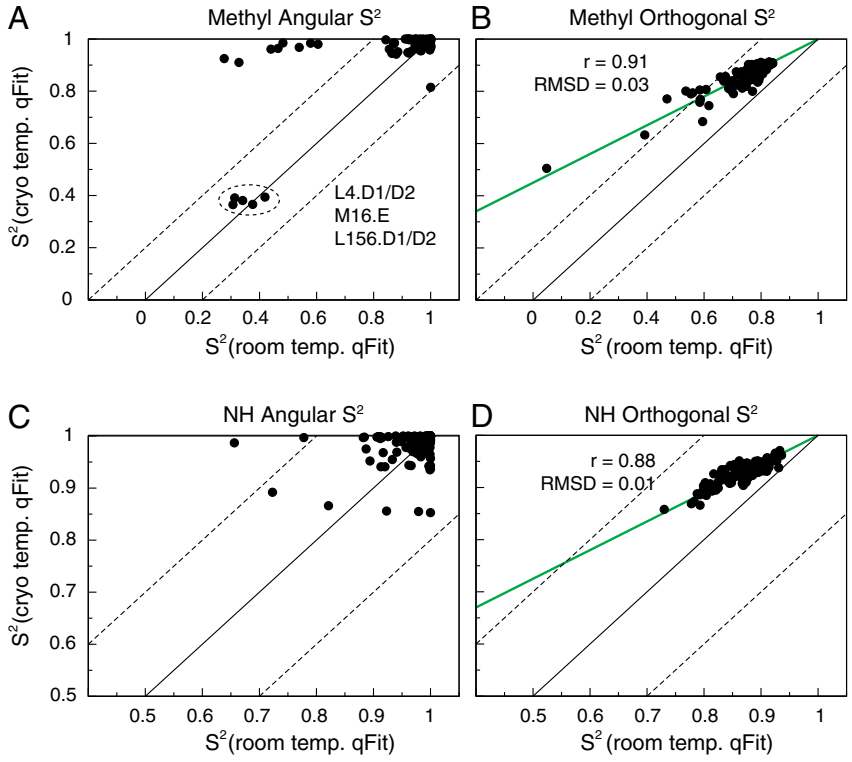

Fig. 5. Correlation plots of room-temperature and cryogenic $S^2_{angular}$ and S^2_{ortho} components of the order parameters for the methyl (*A* and *B*) and NH (*C* and *D*) order parameters. The line of best fit for the temperature dependence of S^2_{ortho} (green) is shown in *B* and *D*.

In contrast, we observed that S^2_{ortho} is temperature sensitive for both side chains and backbone amide groups and that the degree of change for both NH and methyl groups could be fit to the same line ($S^2_{ortho,cryo} = 0.55 * S^2_{ortho,room} + 0.45$) (Fig. 5 *B* and *D*). The ability to model S^2_{ortho} for both groups with the same equation validates the motional models discussed in *Theory*. Note that the orthogonal order parameter did increase for all residues at cryogenic temperature.

Lattice Contacts. In agreement with the work of others (38–40), we found that lattice contacts can directly and indirectly modulate protein dynamics in the crystal. Three residues in the β-CD loop, G67, T68, and D69, which are highly dynamic in solution (30, 31), are motionally restricted in the room-temperature crystal structures (Fig. 4 *A* and *B*). Residues 68–71 make very close backbone and side-chain contact with residues 83–86 and with the side chain of lysine 58 in an adjacent molecule in the crystal lattice; the interactions include both van der Waals contacts and intermolecular backbone and side-chain (K58) hydrogen bonds. Residues 83–86 lie at the C-terminal end of the αE helix and their backbone dynamics appears to be unaffected by the lattice contacts. Omission of residues 67–69 from the analysis improved the agreement between experimental ^{15}N order parameters and those calculated from the room-temperature qFit model (r = 0.67 and rmsd = 0.04). Whereas crystal contacts explain much of the disagreement between solution order parameters and those calculated from the crystal, they also rationalize the decreased motional amplitude of I61 observed in the crystal form. The side chain of I61 is packed against the indole ring of W74, which in turn packs against residues 67–69 in the β-CD loop. This suggests a pathway by which the restriction of motion in the β-CD loop caused by the lattice contacts could be propagated to the I61 side chain. The generally excellent agreement between NMR S^2 values and the order parameters calculated from the room-temperature crystallographic data for the backbone NH, methyl side chains, and the tryptophan side chain indole NH (Fig. 6) suggests that direct refinement may be possible. After exclusion of residues affected by lattice contacts, only two outliers, the methyls of L8 and L112, remain. The potential reasons that these residues show reduced dynamics in the qFit structural model are numerous. L8 is modeled in the structure as the $g-,g+$ ($\chi1$, $\chi2$) rotamer combination, an unfavorable and weakly populated state (41). The side chain can be modeled in alternative noncanonical rotamer combinations without drastically affecting the fit to the electron density (Fig. 7); although the $g-,t$ combination of Fig. 7*C* is rare, it has been observed (41, 42). However, the populations of these $g-,g+$,

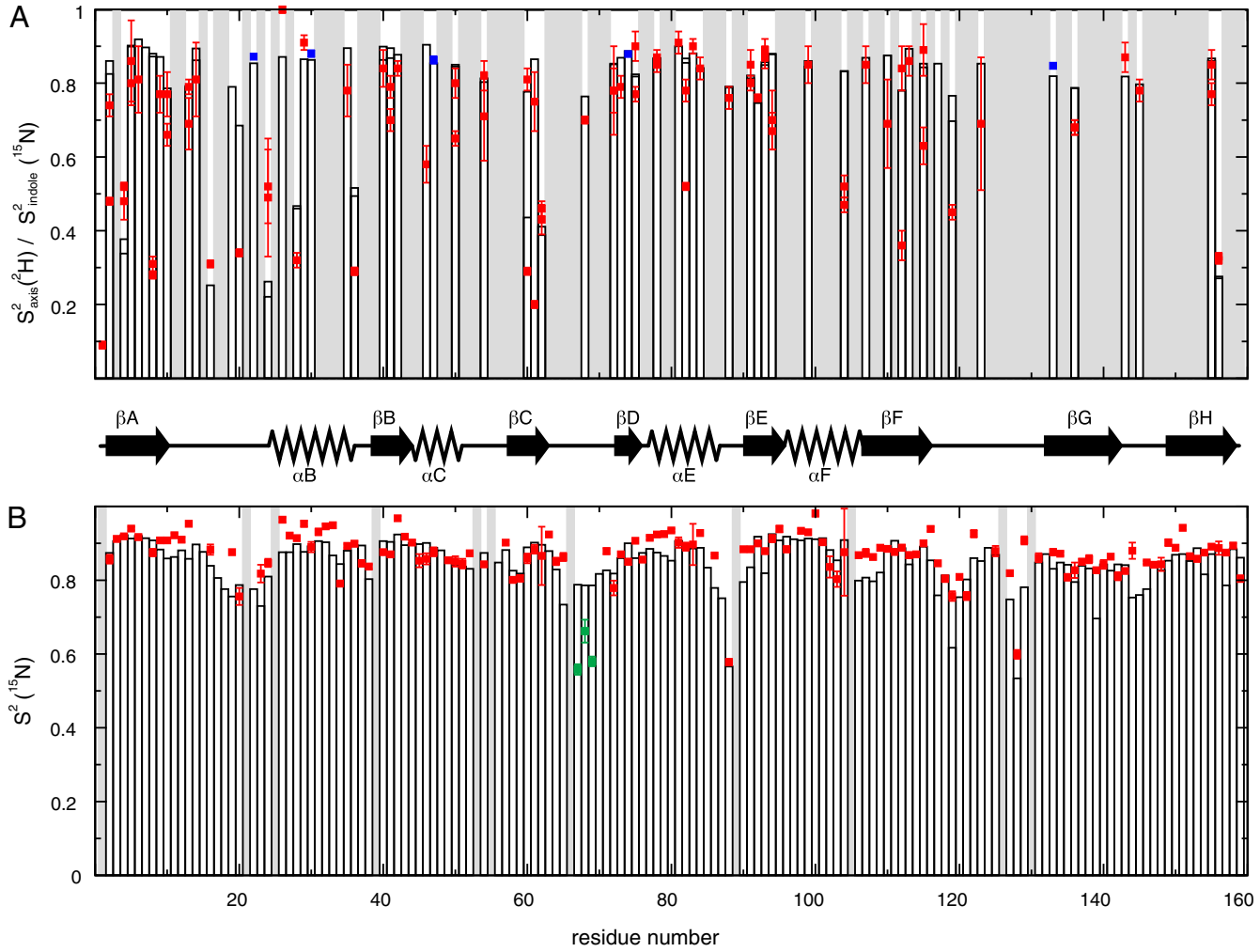

Fig. 6. Experimental and calculated S^2 values from the room-temperature qFit ensemble (bars). Order parameters from all side-chain methyls (red) and Trp indoles (blue) (*A*) and NH groups (*B*) in the protein. Residues that do not contain methyl or amide groups are indicated with gray shading, and residues whose calculated ^{15}N order parameters are affected by lattice contacts are indicated in green.

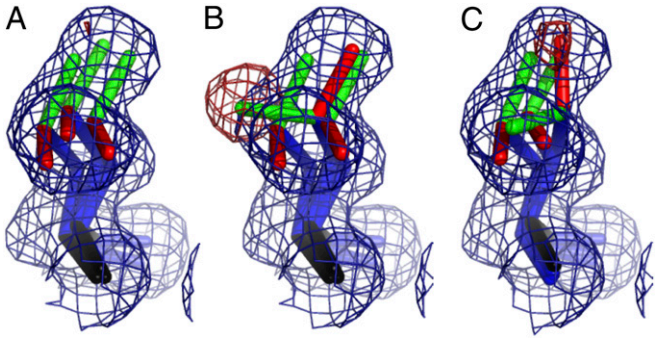

Fig. 7. Alternative models for Leu-8, $2F_oF_c$ electron density around L8 is contoured at 0.3σ (blue) and the difference density is contoured at 3σ (red). qFit model conformational ensemble in the on-rotamer *g*−g+ (χ_1, χ_2) conformation for all states (*A*). One state built in the on-rotamer g−t (*B*). One rotamer built in an off-rotamer g−t conformation (*C*). The backbone is shown as black, side-chain bonds in blue, and bonds to the methyls are identified as green and red.

and *g*−,*t* rotameric states would have to be approximately equal to explain the experimentally observed order parameter. An alternative possibility is that χ_2 averages over all three favorable rotameric states; an ∼16% population of the *g*− and *trans* rotamer states would be sufficient to fit the NMR order parameter. Whereas this residue is packed tightly in the core of the protein, the C^{δ} methyl chemical shifts predict substantial χ_2-rotamer averaging of the L8 side chain (43). For L112 the scenario is similar; this residue is spatially close to two residues, L4 and L156, which both show signs of static disorder. In particular, the methyls of L156 are facing the methyls of L112. Whereas L112 does not display static disorder, it seems likely that the static disorder of L156 in the lattice would further limit the amplitude of motion for L112. Although L112 is not predicted to undergo significant χ_2-rotamer averaging from its chemical shifts, a small population (∼10%) of the χ_2-*trans* rotamer is predicted (43). These two leucines demonstrate the limitations of automatic model building using qFit, and potentially show that noncanonical rotamer states, stabilized by packing and electrostatic contributions, may be present. Moreover, it is clear that the fit of a single rotameric state within the electron density is not proof that multiple alternative rotamer states are not present. The philosophy of the qFit method, and indeed X-ray structure model building in general, is to model the minimal number of states necessary to describe the data. If the population of an additional state is low enough, it may not contribute to the electron density above the level of noise, even though averaging into the state will have a substantial impact on the dynamics observed by NMR relaxation. This work then indicates that in certain cases, when additional dynamic data become available, additional states may need to be modeled.

Discussion

The study of protein dynamics by X-ray diffraction has a long history (44); however, the link between the motional amplitudes and the timescales has remained elusive. Here we have shown that room-temperature crystallographic models provide a quantitative measure of the amplitudes of motions that occur on the ps–ns timescale. In marked contrast, structures determined at cryogenic temperatures fail to capture the amplitudes of motion present in solution. Motional amplitudes from X-ray crystallography are approximated by the B factors, whereas qFit multiconformer models that are composed of multiple states with varying occupancies contain additional motional information.

The motions revealed by the qFit models are distinctly anharmonic and anisotropic in nature. Whereas qFit models are rich in dynamic information, they also capture the inevitable local anisotropy of motions (45–47). qFit and related ensemble methods have an advantage over anisotropic B-factor description because they are not limited to unimodal distributions (48, 49). The qFit model of the DHFR E:FOL:NADP+ complex contains information on the anisotropy and coupling of motions that has been observed from molecular dynamics and NMR measurements (25, 35, 50–52). Within the secondary structure elements of DHFR (Fig. S3), we observed that the crankshaft motion dominates the fluctuations of the peptide planes (27, 51), in which the C^{α} atoms essentially remain fixed and the largest displacements are observed for the carbonyl oxygens and amide protons. We also observed signs of coupling between the motions of peptide planes joined by hydrogen bonds within regular elements of secondary structure (35, 50, 52). Further, motional anisotropy was also evident in side chains, where heterogeneous populations of rotamer states were observed.

The first comparison of B factors and backbone NMR order parameters revealed that a correlation exists (11). However, the agreement was relatively poor and it was suggested that restrictions of motion by the lattice and inflated heterogeneity caused by static disorder heavily influence the B factor. At low resolution, the B factors become less quantitative for assessment of intramolecular dynamics because lattice disorder begins to dominate (44). The poor correlation between B factors and order parameters observed in this early study may have reflected the low resolution of the available data sets (≥2 Å). More recently, Clore and Schwieters (17) were able to refine a small structural ensemble of the third IgG-binding domain of Protein G with residual dipolar couplings, relaxation order parameters, and B factors from a high-resolution (1.1 Å) room-temperature crystal structure, demonstrating for this small globular protein that B factors are consistent with backbone motions on the ps–ns timescale. The temperature at which the diffraction data are acquired can play a major role in the observed heterogeneity (25, 44, 53, 54). Here we have demonstrated that room-temperature diffraction data are critical to obtain a valid description of the structural heterogeneity; correlation with NMR dynamics is reduced when order parameters are calculated from structures or structural ensembles determined at cryogenic temperatures.

The order parameters calculated from multiconformer qFit models, which provide a more realistic description of anharmonic motions and rotameric states, are in overall better agreement with experimental S^2 values than those derived only from the B factors of single-conformer models (Figs. 2 and 4). Methyl S^2_{axis} order parameters are highly sensitive to rotamer averaging, and values less than 0.8 for Ile and Thr, or less than 0.6 for Leu, indicate sampling of multiple rotameric states (55). In the present work, S^2_{axis} values were determined by the standard Lipari–Szabo model from ^{2}H R_1 and $R_{1\rho}$ relaxation, and are a generalized measure of side-chain dynamics on the ps–ns timescale (31). Measurement of additional relaxation rates would permit use of more complex models to separate these motional timescales and provide quantitative insights into ns timescale motions that are likely associated with rotamer jumps (34).

Brüschweiler and Wright proposed the first theoretical connection between order parameters and B factors during the development of the 1D-GAF model (27). This model is very similar to the one that we use here; however, the earlier model overestimates the degree of angular motion encoded in the B factors for both single-conformer and qFit models. This result does not imply that the 1D-GAF model is incorrect; rather, it strengthens the validity of this and related motional models because we find that a single Cartesian variance accurately approximates the angular fluctuations encoded by S^2, rather than the sum of the three Cartesian variances. For single-conformer structural models, local coordinates have been used to characterize the motional amplitudes in proteins (56, 57). Brüschweiler and coworkers have

proposed methods to calculate backbone and side-chain order parameters from atomic coordinates using contact models (12, 13). Whereas these methods do not directly exploit the B factor, they use local contacts to obtain almost equivalent information and perform equally well to the model presented here. One of the drawbacks of these methods is that the relations between the order parameters are empirical and may potentially need recalibrating for each different pair of atoms. A second drawback is that these methods are almost completely insensitive to temperature changes, predicting almost identical order parameters for cryo- and room-temperature structures. When a large number of structures are available the order parameter can be directly calculated from the coordinates (58). Best et al. (18) found that this approach works well for calculating order parameters from molecular dynamics simulations; however, it seems to break down as the ensemble size falls below 25 members. The failure of S^2 to accurately describe the motional amplitudes of small ensembles as observed by Best et al. is consistent with the assumptions of our model and justifies the incorporation of the B-factor contributions via the S^2_{ortho} term for the accurate calculation of the order parameter. Best et al. (18) showed that good agreement is obtained when measured S^2_{axis} values are compared with order parameters calculated from ensembles composed of both alternative crystal forms and structural homologs. The accuracy of their S^2 predictions of order parameters is similar to what we report here. Although their method is limited by the required use of a large number of independently determined structures of high sequence similarity, it does have an advantage in that the impact of crystal contacts can be averaged over a diverse set of crystal lattices.

We have found that lattice contacts in the crystalline state can lead to a dampening of dynamics, compared with solution measurements. This is in accord with previous analyses using contact and Gaussian network models, in which it was demonstrated that crystal contacts can influence local dynamics and B factors (38, 39). In the E:FOL:NADP$^+$ complex of DHFR, the crystal lattice contact between the αE helix and the β-CD loop forms cross-lattice hydrogen bonds that appear to impair backbone motions within the β-CD loop; in contrast the backbone motions of the αE helix are relatively unaffected. This contact reduces the amplitude of motion observed specifically for both the backbone dynamics (residues 67–69) and the side-chain dynamics (I61). In general the β-CD loop is flexible in all DHFR ligand complexes for which NMR relaxation data are available (30). It is unlikely that the temperature difference between the room-temperature diffraction and the NMR measurements contributes to the additional rigidity because the β-EF loop is equally flexible by NMR and its motions are correctly described in the crystal. Thus, lattice contacts appear to be the most plausible origin of the diminished motions in the crystal. Although not attempted here, it may be possible to compensate for the impact of crystal contacts using contact models to correct the B factors of affected residues (39).

By comparing S^2 values calculated from the qFit models and determined from NMR relaxation data, we have been able to diagnose the effects of lattice contacts on the amplitudes of motion of the E:FOL:NADP$^+$ complex of DHFR in the crystalline state. We have also found that static disorder can be identified by comparison of the S^2_{angular} component calculated from room-temperature and cryogenic qFit models. Thus, the combination of room- and cryogenic-temperature qFit coordinates and NMR order parameters facilitates the identification of residues that display modified structural heterogeneity caused indirectly by static disorder of neighboring residues (e.g., L112). Once a qFit model has been validated with NMR order parameters and the residues with anomalous heterogeneity excluded, the room-temperature qFit structures allow us to study the dynamic behavior of the side chains, backbone, and ligands that are not easily amenable to direct NMR relaxation measurements or that would require specialized labeling schemes and experiments—these include nonmethyl side chains, aromatic residues, proline side chains and backbone, and ligands.

In conclusion, side-chain and backbone conformational dynamics of the E:FOL:NADP$^+$ complex of *E. coli* DHFR have been analyzed within a framework that links dynamic order parameters that report on ps–ns timescale motions in solution with qFit models of protein structural heterogeneity in the crystalline state. We find that a simple physical model that incorporates the B factor can accurately predict the backbone and side-chain dynamics of DHFR and that the two methods are fully complementary. Both through the B factors and conformational disorder, the room-temperature qFit structural ensemble accurately reflects the ps–ns timescale motions of the protein backbone and methyl side chains. Regions of the protein involved in crystal lattice contacts are affected by motional dampening; however, the effects are minimal. Finally, the qFit model captures the anisotropic and anharmonic nature of motions, which may prove to be important in linking dynamics to function.

Materials and Methods

Refinement of NH Order Parameters. The NH and tryptophan indole order parameters reported by Osborne (31) were further refined with T1 and T2 measurements made at 500 MHz that were measured on the same sample. The relaxation data sets were analyzed using an axially symmetric diffusion tensor with the amide and indole vector orientations extracted from the DHFR:folate:NADP$^+$ complex structure (PDB ID code 3QL3). The N–H bond length of 1.04 Å and a ^{15}N chemical shift anisotropy (CSA) of −170 ppm were used to remove the impact of libration from the resulting order parameters. For the analysis of the tryptophan indole rings the CSA of −123 ppm was used. Justification of the indole CSA value is given in *SI Text* and Table S1. The relaxation data at multiple fields were fit simultaneously using the extended Lipari–Szabo formalism with an in-house program using the Bayesian information criterion for model selection.

Refinement of Single Structures. The lowest occupancy alternative conformations were manually removed from the coordinate model (PDB ID code) 1RX2 before the datasets were refined with phenix.refine (nightly build 1328) for five rounds with the default strategy and anisotropic B factors. We note that the B factors were not rescaled during or after refinement. The coordinates of the single-conformer models have been deposited with accession numbers PDB ID code 4NX6 (room temperature) and PDB ID code 4NX7 (cryo) and the refinement statistics are given in Table S2.

ACKNOWLEDGMENTS. The authors acknowledge Jack Johnson for helpful discussions. P.E.W. is supported by Grant GM75995 from the National Institutes of Health (NIH) and by the Skaggs Institute for Chemical Biology. H.v.d.B. is supported by the US National Institute of General Medical Sciences Protein Structure Initiative (U54GM094586) at the Joint Center for Structural Genomics and a SLAC National Accelerator Laboratory LDRD (Laboratory Directed Research and Development) Grant SLAC-LDRD-0014-13-2. J.S.F. is supported by Grant DP5 OD009180 from the NIH.

1. Lange OF, et al. (2008) Recognition dynamics up to microseconds revealed from an RDC-derived ubiquitin ensemble in solution. *Science* 320(5882):1471–1475.
2. Boehr DD, McElheny D, Dyson HJ, Wright PE (2006) The dynamic energy landscape of dihydrofolate reductase catalysis. *Science* 313(5793):1638–1642.
3. Eisenmesser EZ, et al. (2005) Intrinsic dynamics of an enzyme underlies catalysis. *Nature* 438(7064):117–121.
4. Gunasekaran K, Ma B, Nussinov R (2004) Is allostery an intrinsic property of all dynamic proteins? *Proteins* 57(3):433–443.
5. Shaanan B, et al. (1992) Combining experimental information from crystal and solution studies: Joint X-ray and NMR refinement. *Science* 257(5072):961–964.
6. Schiffer CA, Huber R, Wüthrich K, van Gunsteren WF (1994) Simultaneous refinement of the structure of BPTI against NMR data measured in solution and X-ray diffraction data measured in single crystals. *J Mol Biol* 241(4):588–599.
7. Brünger AT (1997) X-ray crystallography and NMR reveal complementary views of structure and dynamics. *Nat Struct Biol* 4(Suppl):862–865.
8. Frauenfelder H, Sligar SG, Wolynes PG (1991) The energy landscapes and motions of proteins. *Science* 254(5038):1598–1603.
9. Sherwood D (1976) *Crystals, X-rays, and Proteins* (Longman, London).
10. Hartmann H, et al. (1982) Conformational substates in a protein: Structure and dynamics of metmyoglobin at 80 K. *Proc Natl Acad Sci USA* 79(16):4967–4971.

11. Powers R, Clore GM, Garrett DS, Gronenborn AM (1993) Relationships between the precision of high-resolution protein NMR structures, solution-order parameters, and crystallographic B factors. *J Magn Reson B* 101(3):325–327.
12. Zhang F, Brüschweiler R (2002) Contact model for the prediction of NMR N-H order parameters in globular proteins. *J Am Chem Soc* 124(43):12654–12655.
13. Ming D, Brüschweiler R (2004) Prediction of methyl-side chain dynamics in proteins. *J Biomol NMR* 29(3):363–368.
14. Sunada S, Go N, Koehl P (1996) Calculation of nuclear magnetic resonance order parameters in proteins by normal mode analysis. *J Chem Phys* 104(12):4768–4775.
15. Haliloglu T, Bahar I (1999) Structure-based analysis of protein dynamics: Comparison of theoretical results for hen lysozyme with X-ray diffraction and NMR relaxation data. *Proteins* 37(4):654–667.
16. Diamond R (1990) On the use of normal modes in thermal parameter refinement: Theory and application to the bovine pancreatic trypsin inhibitor. *Acta Crystallogr A* 46(Pt 6):425–435.
17. Clore GM, Schwieters CD (2006) Concordance of residual dipolar couplings, backbone order parameters and crystallographic B-factors for a small alpha/beta protein: A unified picture of high probability, fast atomic motions in proteins. *J Mol Biol* 355(5): 879–886.
18. Best RB, Lindorff-Larsen K, DePristo MA, Vendruscolo M (2006) Relation between native ensembles and experimental structures of proteins. *Proc Natl Acad Sci USA* 103 (29):10901–10906.
19. Zinkevich T, Chevelkov V, Reif B, Saalwächter K, Krushelnitsky A (2013) Internal protein dynamics on ps to μs timescales as studied by multi-frequency (15)N solid-state NMR relaxation. *J Biomol NMR* 57(3):219–235.
20. Nickels JD, García Sakai V, Sokolov AP (2013) Dynamics in protein powders on the nanosecond-picosecond time scale are dominated by localized motions. *J Phys Chem B* 117(39):11548–11555.
21. Agarwal V, Xue Y, Reif B, Skrynnikov NR (2008) Protein side-chain dynamics as observed by solution- and solid-state NMR spectroscopy: A similarity revealed. *J Am Chem Soc* 130(49):16611–16621.
22. Reif B, et al. (2006) Protein side-chain dynamics observed by solution- and solid-state NMR: Comparative analysis of methyl 2H relaxation data. *J Am Chem Soc* 128(38): 12354–12355.
23. Haller JD, Schanda P (2013) Amplitudes and time scales of picosecond-to-microsecond motion in proteins studied by solid-state NMR: A critical evaluation of experimental approaches and application to crystalline ubiquitin. *J Biomol NMR* 57(3):263–280.
24. van den Bedem H, Dhanik A, Latombe JC, Deacon AM (2009) Modeling discrete heterogeneity in X-ray diffraction data by fitting multi-conformers. *Acta Crystallogr D Biol Crystallogr* 65(Pt 10):1107–1117.
25. van den Bedem H, Bhabha G, Yang K, Wright PE, Fraser JS (2013) Automated identification of functional dynamic contact networks from X-ray crystallography. *Nat Methods* 10(9):896–902.
26. Lipari G, Szabo A (1982) Model-free approach to the interpretation of nuclear magnetic resonance relaxation in macromolecules. 1. Theory and range of validity. *J Am Chem Soc* 104(17):4546–4559.
27. Brüschweiler R, Wright PE (1994) NMR order parameters of biomolecules: A new analytical representation and application to the Gaussian axial fluctuation model. *J Am Chem Soc* 116(18):8426–8427.
28. Busing WR, Levy HA (1964) The effect of thermal motion on the estimation of bond lengths from diffraction measurements. *Acta Crystallogr* 17(2):142–146.
29. Bremi T, Brüschweiler R (1997) Locally anisotropic internal polypeptide backbone dynamics by NMR relaxation. *J Am Chem Soc* 119(28):6672–6673.
30. Osborne MJ, Schnell J, Benkovic SJ, Dyson HJ, Wright PE (2001) Backbone dynamics in dihydrofolate reductase complexes: Role of loop flexibility in the catalytic mechanism. *Biochemistry* 40(33):9846–9859.
31. Schnell JR, Dyson HJ, Wright PE (2004) Effect of cofactor binding and loop conformation on side chain methyl dynamics in dihydrofolate reductase. *Biochemistry* 43(2):374–383.
32. Nicholson LK, et al. (1992) Dynamics of methyl groups in proteins as studied by proton-detected 13C NMR spectroscopy. Application to the leucine residues of staphylococcal nuclease. *Biochemistry* 31(23):5253–5263.
33. Muhandiram DR, Yamazaki T, Sykes BD, Kay LE (1995) Measurement of 2H T1 and T1. rho. Relaxation times in uniformly 13C-labeled and fractionally 2H-labeled proteins in solution. *J Am Chem Soc* 117(46):11536–11544.
34. Skrynnikov NR, Millet O, Kay LE (2002) Deuterium spin probes of side-chain dynamics in proteins. 2. Spectral density mapping and identification of nanosecond time-scale side-chain motions. *J Am Chem Soc* 124(22):6449–6460.
35. Bouvignies G, et al. (2005) Identification of slow correlated motions in proteins using residual dipolar and hydrogen-bond scalar couplings. *Proc Natl Acad Sci USA* 102(39): 13885–13890.
36. Tilton RFJ, Jr., Dewan JC, Petsko GA (1992) Effects of temperature on protein structure and dynamics: X-ray crystallographic studies of the protein ribonuclease-A at nine different temperatures from 98 to 320 K. *Biochemistry* 31(9):2469–2481.
37. Halle B (2004) Biomolecular cryocrystallography: Structural changes during flash-cooling. *Proc Natl Acad Sci USA* 101(14):4793–4798.
38. Kundu S, Melton JS, Sorensen DC, Phillips GNJ, Jr. (2002) Dynamics of proteins in crystals: Comparison of experiment with simple models. *Biophys J* 83(2):723–732.
39. Li DW, Brüschweiler R (2009) All-atom contact model for understanding protein dynamics from crystallographic B-factors. *Biophys J* 96(8):3074–3081.
40. Jacobson MP, Friesner RA, Xiang Z, Honig B (2002) On the role of the crystal environment in determining protein side-chain conformations. *J Mol Biol* 320(3):597–608.
41. Shapovalov MV, Dunbrack RLJ, Jr. (2011) A smoothed backbone-dependent rotamer library for proteins derived from adaptive kernel density estimates and regressions. *Structure* 19(6):844–858.
42. Petrella RJ, Karplus M (2001) The energetics of off-rotamer protein side-chain conformations. *J Mol Biol* 312(5):1161–1175.
43. Tuttle LM, Dyson HJ, Wright PE (2013) Side-chain conformational heterogeneity of intermediates in the Escherichia coli dihydrofolate reductase catalytic cycle. *Biochemistry* 52(20):3464–3477.
44. Petsko GA, Ringe D (1984) Fluctuations in protein structure from X-ray diffraction. *Annu Rev Biophys Bioeng* 13:331–371.
45. García AE (1992) Large-amplitude nonlinear motions in proteins. *Phys Rev Lett* 68(17): 2696–2699.
46. Atilgan AR, et al. (2001) Anisotropy of fluctuation dynamics of proteins with an elastic network model. *Biophys J* 80(1):505–515.
47. Kuriyan J, Petsko GA, Levy RM, Karplus M (1986) Effect of anisotropy and anharmonicity on protein crystallographic refinement. An evaluation by molecular dynamics. *J Mol Biol* 190(2):227–254.
48. Burnley BT, Afonine PV, Adams PD, Gros P (2012) Modelling dynamics in protein crystal structures by ensemble refinement. *Elife* 1:e00311.
49. Nwachukwu JC, et al. (2013) Improved crystallographic structures using extensive combinatorial refinement. *Structure* 21(11):1923–1930.
50. Fenwick RB, et al. (2011) Weak long-range correlated motions in a surface patch of ubiquitin involved in molecular recognition. *J Am Chem Soc* 133(27):10336–10339.
51. Fadel AR, Jin DQ, Montelione GT, Levy RM (1995) Crankshaft motions of the polypeptide backbone in molecular dynamics simulations of human type-alpha transforming growth factor. *J Biomol NMR* 6(2):221–226.
52. Vögeli B, Kazemi S, Güntert P, Riek R (2012) Spatial elucidation of motion in proteins by ensemble-based structure calculation using exact NOEs. *Nat Struct Mol Biol* 19(10): 1053–1057.
53. Fraser JS, et al. (2009) Hidden alternative structures of proline isomerase essential for catalysis. *Nature* 462(7273):669–673.
54. Fraser JS, et al. (2011) Accessing protein conformational ensembles using room-temperature X-ray crystallography. *Proc Natl Acad Sci USA* 108(39):16247–16252.
55. Hu H, Hermans J, Lee AL (2005) Relating side-chain mobility in proteins to rotameric transitions: Insights from molecular dynamics simulations and NMR. *J Biomol NMR* 32 (2):151–162.
56. Jacobs DJ, Rader AJ, Kuhn LA, Thorpe MF (2001) Protein flexibility predictions using graph theory. *Proteins* 44(2):150–165.
57. Halle B (2002) Flexibility and packing in proteins. *Proc Natl Acad Sci USA* 99(3): 1274–1279.
58. Henry ER, Szabo A (1985) Influence of vibrational motion on solid state line shapes and NMR relaxation. *J Chem Phys* 82(11):4753–4761.

Supporting Information

Fenwick et al. 10.1073/pnas.1323440111

SI Text

The chemical shift anisotropy (CSA) value for indole of the tryptophan side chain was calculated using the measured values of CSA from solution (1) and solid-state NMR (2–3), assuming that the scaling of the indole CSA is equivalent to that observed for the peptide backbone. This gave a value of −110 ppm for the CSA of the indole (Table S1). The indole CSA was then further scaled (4) to account for the asymmetry value of 0.82 by a factor = $\sqrt{(1+\eta^2/3)}$, to give a final effective value of −122 ppm.

1. Cornilescu G, Bax A (2000) Measurement of proton, nitrogen, and carbonyl chemical shielding anisotropies in a protein dissolved in a dilute liquid crystalline phase. *J Am Chem Soc* 122(41):10143–10154.
2. Ramamoorthy A, Wu CH, Opella SJ (1997) Magnitudes and orientations of the principal elements of the 1H chemical shift, 1H-15N dipolar coupling, and 15N chemical shift interaction tensors in 15Nε1-tryptophan and 15Nπ-histidine side chains determined by three-dimensional solid-state NMR spectroscopy of polycrystalline samples. *J Am Chem Soc* 119(43):10479–10486.
3. Wu CH, Ramamoorthy A, Gierasch LM, Opella SJ (1995) Simultaneous characterization of the amide 1H chemical shift, 1H-15N dipolar, and 15N chemical shift interaction tensors in a peptide bond by three-dimensional solid-state NMR spectroscopy. *J Am Chem Soc* 117(22):6148–6149.
4. Kowalewski J, Mäler L (2006) *Nuclear Spin Relaxation in Liquids: Theory, Experiments, and Applications* (Taylor & Francis, New York).

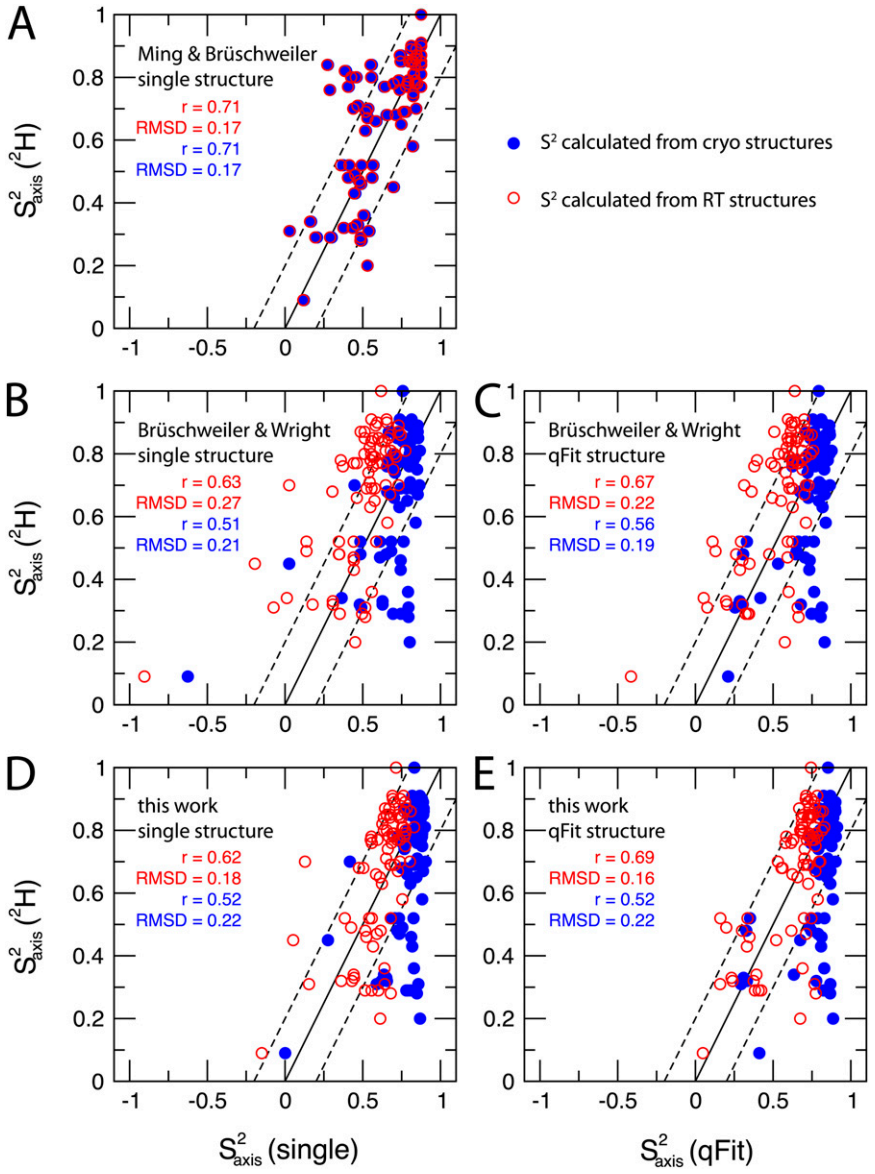

Fig. S1. Comparison of side-chain methyl order parameters using different models. The contact model of Ming and Brüschweiler (*A*) for the single-conformer structure, from the original B-factor framework of Brüschweiler and Wright (*B* and *C*) for single and qFit structures, respectively, and the model proposed in this work (*D* and *E*) for single and qFit structures, respectively.

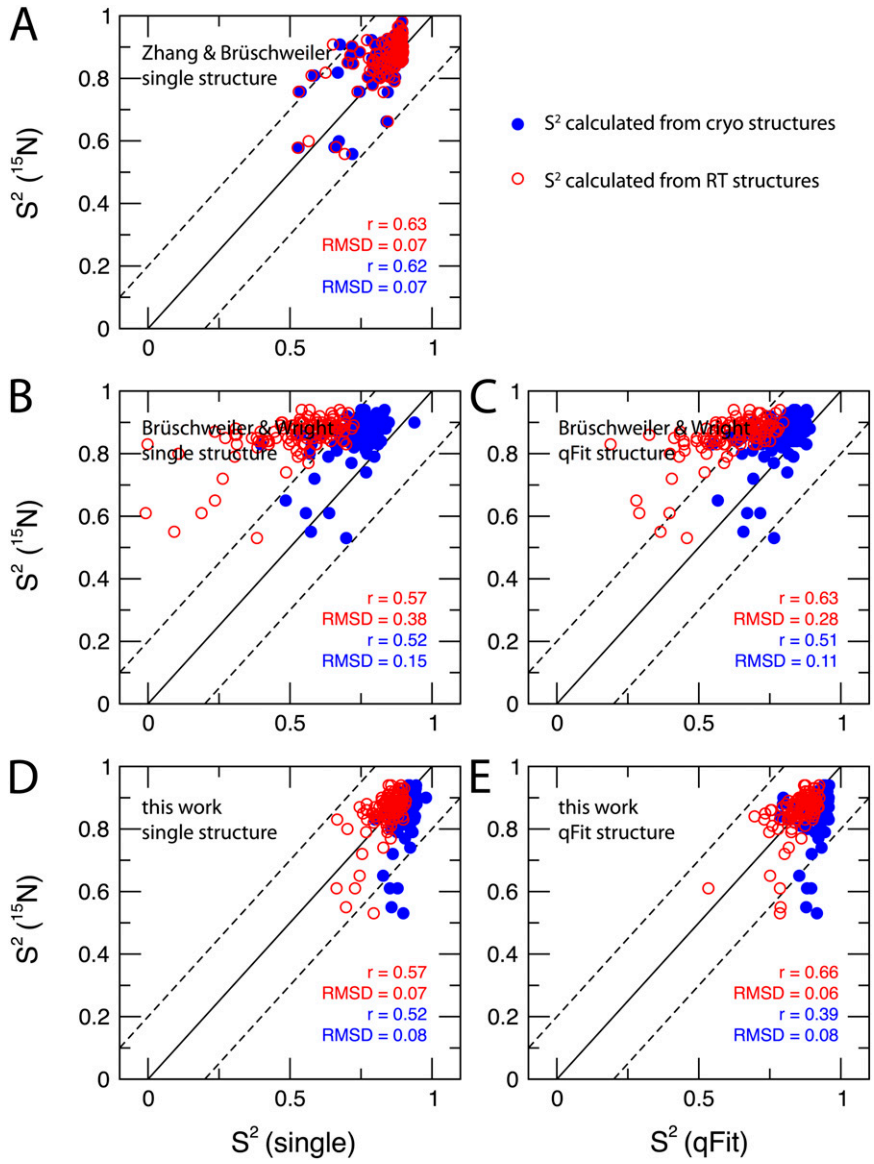

Fig. S2. Comparison of backbone NH order parameters using different models. The contact model of Ming and Brüschweiler (*A*) for the single-conformer structure, from the original B-factor framework of Brüschweiler and Wright (*B* and *C*) for single and qFit structures, respectively, and the model proposed in this work (*D* and *E*) for single and qFit structures, respectively.

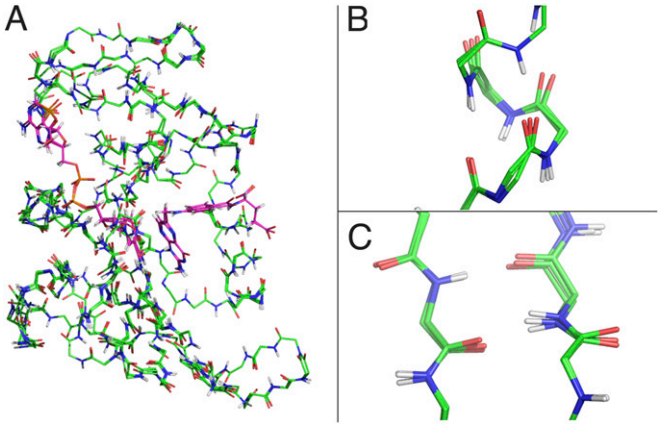

Fig. S3. Room-temperature qFit ensemble for the DHFR:folate:NADP$^+$ complex showing the anisotropic motion of the backbone in secondary structure elements. The qFit ensemble (green) with the ligands colored in pink (*A*). The crankshaft motion of the peptide plane, within the helix αB (*B*) and within the central β-sheet (*C*) for strands βF and βH, where the peptide plane is observed to rotate around the $C^{\alpha}_{i-1} - C^{\alpha}_{i}$ axis. The observed tilting of the peptide planes is caused by the anticorrelated rotations of ψ_{i-1} with ϕ_i and the motion is synonymous with the crankshaft motion and the γ-motion within the 3D Gaussian axial fluctuation (3D-GAF) model.

Table S1. Published values of the CSA for Trp indoles and the peptide amide

Trp CSA	$\Delta\sigma$, ppm	η	$\Delta\sigma$ eff., ppm
Solid-state peptide (3)	−147	0.13	−147
Solution-state peptide (1)	−170	0.16	−171
Solid-state indole (2)	−95	0.82	−105
Solution-state indole	−110	0.82	−122

Table S2. Data collection and refinement statistics

Refinement	Room temperature, Protein Data Bank (PDB) ID code 4NX6	Cryogenic, PDB ID code 4NX7
Resolution (Å)	41.34–1.35 (1.40–1.35)	40.77–1.15 (1.19–1.15)
Space group	P 21 21 21	P 21 21 21
Unit cell	34.3 45.5 98.9 90 90 90	34.0 44.8 98.2 90 90 90
R-work	0.144 (0.214)	0.138 (0.130)
R-free	0.189 (0.341)	0.169 (0.191)
Number of nonhydrogen atoms	1,518	1,728
Macromolecules	1,268	1,268
Ligands	82	82
Water	168	378
Protein residues	159	159
rms, bonds	0.016	0.021
rms, angles	1.41	1.97
Ramachandran favored, %	99	99
Ramachandran outliers, %	0	0
Clashscore	5.35	14.1
Average B factor	18.0	12.2
Macromolecules	16.3	9.6
Ligands	15.1	9.4
Solvent	32.1	21.3

Statistics for the highest-resolution shell are shown in parentheses.